Radiology

Time-Dependent Diffusion MRI Helps Predict Molecular Subtypes and Treatment Response to Neoadjuvant Chemotherapy in Breast Cancer

Xiaoxia Wang, MS* • Ruicheng Ba, MS* • Yao Huang, MS • Ying Cao, MS • Huifang Chen, MS • Hanshan Xu, MS • Hesong Shen, MS • Daihong Liu, MD • Haiping Huang, MS • Ting Yin, PHD • Dan Wu, PHD** • Jiuquan Zhang, MD**

From the Department of Radiology, Chongqing University Cancer Hospital, Chongqing Key Laboratory for Intelligent Oncology in Breast Cancer (iCQBC), No. 181 Hanyu Road, Shapingba, Chongqing 400030, China (X.W., H.C., H.X., H.S., D.L., J.Z.); Department of Biomedical Engineering, Key Laboratory for Biomedical Engineering of Ministry of Education, Zhejiang University College of Biomedical Engineering and Instrument Science, Hangzhou China (R.B., D.W.); Chongqing University School of Medicine, Chongqing, China (Y.H., Y.C.); Department of Pathology, Chongqing University Cancer Hospital, Chongqing, China (H.H.); and MR Collaborations, Siemens Healthineers, Chengdu, China (T.Y.). Received January 29, 2024; revision requested March 5; revision received June 23; accepted July 10. **Address correspondence to** J.Z. (email: *zhangjq_radiol@foxmail.com*).

* X.W. and R.B. contributed equally to this work.

** D.W. and J.Z. are co-senior authors.

Conflicts of interest are listed at the end of this article.

See also the editorial by Partridge and Xu in this issue.

Background: Time-dependent diffusion MRI has the potential to help characterize tumor cell properties; however, to the knowledge of the authors, its usefulness for breast cancer diagnosis and prognostic evaluation is unknown.

Purpose: To investigate the clinical value of time-dependent diffusion MRI–based microstructural mapping for noninvasive prediction of molecular subtypes and pathologic complete response (pCR) in participants with breast cancer.

Materials and methods: Participants with invasive breast cancer who underwent pretreatment with time-dependent diffusion MRI between February 2021 and May 2023 were prospectively enrolled. Four microstructural parameters were estimated using the IMPULSED method (a form of time-dependent diffusion MRI), along with three apparent diffusion coefficient (ADC) measurements and a relative ADC diffusion-weighted imaging parameter. Multivariable logistic regression analysis was used to identify parameters associated with each molecular subtype and pCR. A predictive model based on associated parameters was constructed, and its performance was assessed using the area under the receiver operating characteristic curve (AUC) and compared by using the DeLong test. The time-dependent diffusion MRI parameters were validated based on correlation with pathologic measurements.

Results: The analysis included 408 participants with breast cancer (mean age, 51.9 years ± 9.1 [SD]). Of these, 221 participants were administered neoadjuvant chemotherapy and 54 (24.4%) achieved pCR. The time-dependent diffusion MRI parameters showed reasonable performance in helping to identify luminal A (AUC, 0.70), luminal B (AUC, 0.78), and triple-negative breast cancer (AUC, 0.72) subtypes and high performance for human epidermal growth factor receptor 2 *(HER2)*-enriched breast cancer (AUC, 0.85), outperforming ADC measurements (all $P < .05$). Progesterone receptor status (odds ratio [OR], 0.08; $P = .02$), *HER2* status (OR, 3.36; $P = .009$), and the cellularity index (OR, 0.01; $P = .02$) were independently associated with the odds of achieving pCR. The combined model showed high performance for predicting pCR (AUC, 0.88), outperforming ADC measurements and the clinical-pathologic model (AUC, 0.73 and 0.79, respectively; $P < .001$). The time-dependent diffusion MRI–estimated parameters correlated well with the pathologic measurements ($n = 100$; $r = 0.67–0.81$; $P < .001$).

Conclusion: Time-dependent diffusion MRI–based microstructural mapping was an effective method for helping to predict molecular subtypes and pCR to neoadjuvant chemotherapy in participants with breast cancer.

© RSNA, 2024

Supplemental material is available for this article.

B reast cancer is a heterogeneous disease with various molecular subtypes, and patients have varied responses to therapy (1). These molecular subtypes are closely associated with the pathologic characteristics in each breast cancer (2), such as tumor cellularity, and have a vital role in guiding treatment strategies. Luminal A subtype is usually treated with endocrine therapy only, whereas the addition of cytotoxic therapy is indicated for patients with luminal B and triple-negative breast cancer (TNBC). Human epidermal growth factor receptor 2

(HER2)-enriched subtype often requires anti-*HER2* therapy. Immunohistochemical determination of molecular subtypes is sensitive to errors due to intratumoral heterogeneity and limited tissue sampling. In addition, the tumor subtypes may change over time and with treatment. This limits the clinical application of invasive biopsy sampling, particularly when considering multiple sites and points. Therefore, there is an urgent need for noninvasive detection methods to help evaluate molecular subtypes.

Abbreviations

ADC = apparent diffusion coefficient, $ADC_{50 Hz}$ = ADC measurement at 50 Hz, $ADC_{25 Hz}$ = ADC measurement at 25 Hz, AUC = area under the receiver operating characteristic curve, *HER2* = human epidermal growth factor receptor 2, OR = odds ratio, pCR = pathologic complete response, TNBC = triple-negative breast cancer

Summary

Time-dependent diffusion MRI–based microstructural mapping was shown to be an effective method in helping to identify molecular subtypes and predict pathologic complete response to neoadjuvant chemotherapy in participants with breast cancer.

Key Results

- In a prospective study of 408 participants with breast cancer, time-dependent diffusion MRI microstructural parameters helped identify molecular subtypes (area under the receiver operating characteristic curve [AUC] range, 0.70–0.85).
- A model combining progesterone receptor, human epidermal growth factor receptor 2, and time-dependent diffusion MRI microstructural parameters achieved good performance for predicting pathologic complete response (AUC, 0.88) and was better than conventional diffusion-weighted MRI and clinical-pathologic models (*P* < .001).
- Time-dependent diffusion MRI–based microstructural parameters and pathologic analysis–based microstructural properties were closely correlated (*r* = 0.67–0.81).

Neoadjuvant chemotherapy is used widely (3), and pathologic complete response (pCR) to neoadjuvant chemotherapy serves as a surrogate marker for long-term survival. Unfortunately, pCR rates after neoadjuvant chemotherapy differ according to tumor subtype, ranging from 0.3% to 50.3% (4), with a greater risk of recurrence in patients who do not achieve pCR. Early prediction of pCR can assist clinicians in adjusting therapy to avoid toxic adverse effects and to improve survival. To the knowledge of the authors, there are no standard methods available that can accurately predict pCR before neoadjuvant chemotherapy is administered.

Diffusion-weighted imaging is a widely used imaging technique that depicts the behavior of restrictive water diffusion in biologic tissues by using different diffusion weights (known as *q*-spaces) (5). It shows potential in the noninvasive characterization of breast cancer subtypes (6) and detection of early pathologic changes in tumor treatment (7). However, there is an overlap in apparent diffusion coefficient (ADC) values across classification categories, possibly because the ADC only describes the overall water diffusion rate and cannot provide specific microstructural information about tumor pathologic structure (8).

Time-dependent diffusion MRI using varying diffusion times (known as *t*-space) can characterize microstructural properties, such as the cell diameter, intracellular fraction (referred to as f_{in}), and cellularity, which cannot be measured with conventional diffusion-weighted imaging (9). Specifically, the previously developed IMPULSED method is a unique time-dependent diffusion MRI technique that leverages both q-space and t-space and establishes analytical biophysical models to characterize microstructural properties (10,11) that can be implemented on clinical scanners (12). The clinical feasibility of time-dependent diffusion MRI has been explored in breast tumors (12–14); for example, Ba et al (13) reported the feasibility of distinguishing immunohistochemical phenotypes of breast tumors using the time-dependent diffusion MRI approach. Nevertheless, the clinical value of time-dependent diffusion MRI in imaging breast tumors remains to be elucidated. Therefore, large-scale studies are needed to further validate the performance of time-dependent diffusion MRI in helping to predict molecular subtypes and pCR.

We hypothesized that time-dependent diffusion MRI methods could help to characterize microstructural properties, thus enabling the prediction of molecular subtypes and pCR. The aim of this study was to investigate the clinical value of time-dependent diffusion MRI–based microstructural mapping for noninvasive prediction of molecular subtypes and pCR in participants with breast cancer.

Materials and Methods

Study Sample

This prospective study was conducted by following the Declaration of Helsinki and approved by the institutional review board of the local hospital (Chongqing University Cancer Hospital, Chongqing, China). Informed consent was obtained from all participants. Consecutive participants with lesions that were Breast Imaging Reporting and Data System category 4 or greater and detected at mammography and/or US (category 4, 184 participants; category 5, 338 participants) were prospectively recruited to the study and invited to undergo breast MRI between February 2021 and May 2023. The inclusion criteria were as follows: participants underwent pretreatment breast MRI, including time-dependent diffusion MRI and routine scans; unilateral primary invasive breast cancer verified at histopathologic analysis; clinical and immunohistochemical data were available; and pCR status confirmed at pathologic examination in participants undergoing neoadjuvant chemotherapy. The exclusion criterion was the inability to obtain measurements because of motion artifacts compromising the MRI scan quality (*n* = 27); and surgical procedures were performed at an external institution, with pCR status not obtained (*n* = 13). The participant enrollment study flowchart is shown in Figure 1.

Data Acquisition at MRI

With the participant in the prone position, 3-T MRI (Magnetom Prisma; Siemens Healthineers) was performed with a dedicated 16-channel breast coil. An oscillating gradient spin-echo sequence, developed in-house (13) with trapezoid-cosine gradients and pulsed gradient spin echo, was implemented with two-dimensional echo-planar image acquisition. Oscillating gradient spin-echo data were acquired at 25 Hz (effective diffusion time, 10 msec; one cycle; *b* values, 0; 250, 500, 750, and 1000 sec/mm²) and 50 Hz (effective diffusion time, 5 msec; two cycles; *b* values, 0, 250, and 500 sec/mm²). Pulsed gradient spin-echo images were acquired with diffusion duration (10 msec) and separation (30 msec) at *b* values of 0, 250, 500, 750, and 1000 sec/mm². See Appendix S1 for details.

Image Analysis

Time-dependent diffusion MRI signals were normalized by dividing them by the *b* value of 0 sec/mm² signals. The normalized signals were then fitted with the monoexponential model to calculate ADC values and the limited spectrally edited diffusion
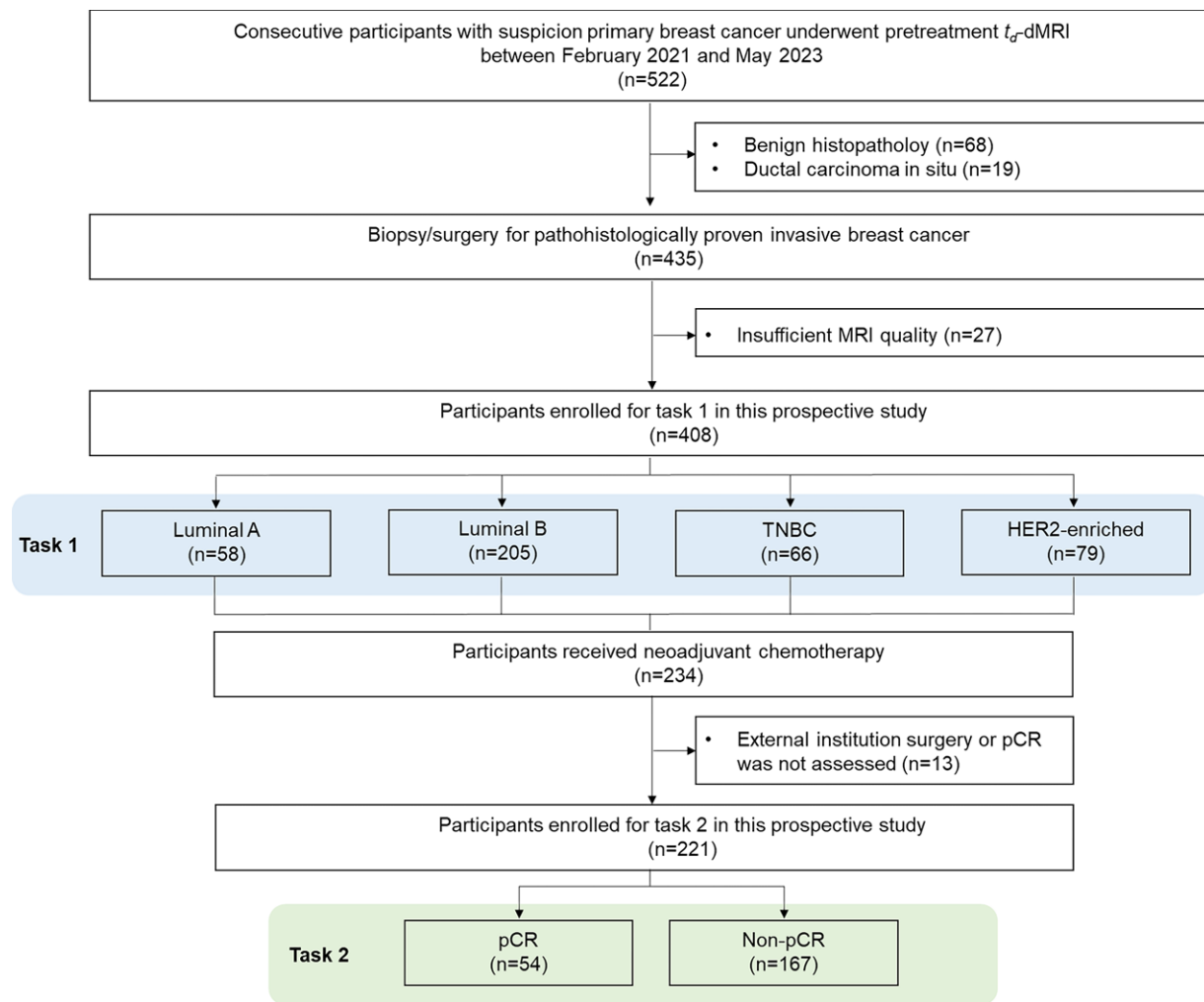
Figure 1: Flowchart shows participant enrollment. HER2 = human epidermal growth factor receptor 2, pCR = pathologic complete response, t_d-dMRI = time-dependent diffusion MRI, TNBC = triple-negative breast cancer.

(known as IMPULSED) method to estimate microstructural properties (15) (Appendix S1). An experienced radiologist (X.W., with 10 years of experience), blinded to participant data, manually delineated regions of interest of breast tumor tissue on each section based on diffusion-weighted images. The surrounding tissue was carefully excluded. The fitted microstructural parameters (diameter, intracellular fraction, extracellular diffusivity, and cellularity), ADCs at different diffusion times (pulsed gradient spin-echo ADC, ADC measurement at 25 Hz [$ADC_{25\ Hz}$], and ADC measurement at 50 Hz [$ADC_{50\ Hz}$]), and relative ADC change (16) were calculated in a voxelwise manner and averaged within each tumor region of interest.

Histopathologic Assessment and Correlation with MRI

Based on the immunohistochemistry or fluorescence in situ hybridization results for estrogen receptor, progesterone receptor, HER2, and Ki-67, participants were classified into luminal A, luminal B, HER2-enriched, and TNBC subtypes (17,18) (Appendix S1). Treatment response was evaluated by a binary indicator of pCR or non-pCR confirmed in a surgical specimen after neoadjuvant chemotherapy; pCR was defined as the absence of residual invasive carcinoma (residual ductal carcinoma in situ could be present) and the absence of axillary lymph node invasion (pathologic stage ypT0/isN0).

Histopathologic slides were interpreted by a pathologist (H.H., with 15 years of experience) who was blinded to the findings at MRI. The nuclei in each whole-slide image were segmented by using a pretrained conditional generative adversarial network (19). The volume-weighted diameter of the nuclei was calculated as $d_{nuclei} = \sum_n d_n^4 / \sum_n d_n^3$, where n represents the cell number, d is diameter, and Σ is the sum, and the nucleus diameter (d_{nuclei}) was scaled to the cell diameter based on a scaling factor of 1.8 (13). Pathologic analysis–based intracellular fraction was calculated as $(\sum_n A_{nuclei} / A_{tissue})^{3/2}$, where A_{tissue} is the area of the whole tissue and A_{nuclei} is the area of the whole nuclei. The pathologic cellularity was calculated as follows: (pathologic cellularity = [intracellular fraction pathologic structure/diameter pathologic structure] × 100).

Statistical Analysis

Statistical analyses were performed (Y.H., with 5 years of experience) using software (SPSS, version 26, IBM; MedCalc, version 20.022, MedCalc Software). The null hypothesis of an area under the receiver operating characteristic curve (AUC) was 0.50 and the alternate hypothesis of an AUC was 0.70; statistical power was 90%; the average proportions were 55%, 15%, 15%, and 15% for luminal A, luminal B,

Table 1: Clinical-Pathologic Participant Characteristics

Characteristic	All (n = 408)	Luminal A (n = 58)	Luminal B (n = 205)	TNBC (n = 66)	HER2-enriched (n = 79)	P Value
Mean age (y)*	51.9 ± 9.1	50.9 ± 9.5	51.2 ± 9.2	53.8 ± 10.2	52.9 ± 7.4	.19†
Age						.7‡
≤45 years	71 (17.4)	13 (22.4)	40 (17.6)	12 (18.2)	6 (7.6)	...
>45 years	337 (82.6)	45 (77.6)	165 (80.5)	54 (81.8)	73 (92.4)	...
Body mass index (kg/m²)*	25.02 ± 3.57	24.81 ± 2.80	25.39 ± 3.78	24.97 ± 3.91	24.28 ± 3.09	.12†
Menstruation status						.19‡
Premenopausal	113 (27.7)	14 (24.1)	51 (24.9)	25 (37.8)	23 (29.1)	...
Postmenopausal	295 (72.3)	44 (75.9)	154 (75.1)	41 (62.2)	56 (70.9)	...
T stage						.01§
1	68 (16.7)	19 (32.8)	26 (12.7)	9 (13.6)	14 (17.7)	...
2	202 (49.5)	17 (29.3)	112 (54.6)	34 (51.5)	39 (49.4)	...
3	39 (9.6)	4 (6.9)	17 (8.3)	7 (10.6)	11 (13.9)	...
4	99 (24.2)	18 (31.0)	50 (24.4)	16 (24.3)	15 (19.0)	...
N stage						.8‡
0	123 (30.1)	26 (44.8)	57 (27.8)	19 (28.7)	21 (26.6)	...
1	113 (27.7)	15 (25.9)	59 (28.8)	16 (24.3)	23 (29.1)	...
2	114 (27.9)	9 (15.5)	66 (32.2)	21 (31.8)	18 (22.8)	...
3	58 (14.3)	8 (13.8)	23 (11.2)	10 (15.2)	17 (21.5)	...
M stage						.74§
0	387 (94.9)	56 (96.6)	195 (95.1)	63 (95.5)	73 (92.4)	...
1	21 (5.1)	2 (3.4)	10 (4.9)	3 (4.5)	6 (7.6)	...
Clinical stage						.14§
I	45 (11.0)	13 (22.4)	17 (8.3)	5 (7.6)	10 (12.7)	...
II	144 (35.3)	16 (27.6)	75 (36.6)	22 (33.3)	31 (39.2)	...
III	198 (48.5)	27 (46.6)	103 (50.2)	36 (54.6)	32 (40.5)	...
IV	21 (5.2)	2 (3.4)	10 (4.9)	3 (4.5)	6 (7.6)	...

Note.—Unless otherwise indicated, data are numbers of participants; data in parentheses are percentages. HER2 = human epidermal growth factor receptor 2, TNBC = triple-negative breast cancer.

* Data are means ± SDs for continuous variables.

† One-way analysis of variance.

‡ χ^2 test.

§ Fisher exact test.

TNBC, and HER2-enriched subtypes, and 25% and 75% for pCR and non-pCR groups, respectively. The minimum required samples were 173 patients (task 1) and 116 patients (task 2). Continuous variables are reported as means ± SDs and categorical variables are reported as frequencies with percentages. Group comparisons were analyzed using independent t tests or Mann-Whitney U tests for continuous variables. Categorical variables were compared using the χ^2 test or Fisher exact test. Comparisons of time-dependent diffusion MRI microstructural parameter differences among the subtypes were performed using one-way analysis of variance followed by pairwise t tests with Bonferroni correction. Univariable and multivariable logistic regression analyses were performed to assess the associations between variables associated with each molecular subtype and pCR. The AUC, accuracy, specificity, sensitivity, negative predictive value, and positive predictive value were used to evaluate the diagnostic performance. Bootstrapped CIs and odds ratios (ORs) were calculated. The optimal cutoff value was determined according to the Youden index. The DeLong test was used to compare the model performance. Correlations analysis was assessed using the Pearson correlation coefficient (r coefficient). Two-tailed $P < .05$ was considered to indicate statistical significance.

Results

Participant Characteristics
In total, 408 participants (mean age, 51.9 years ± 9.1 [SD]) with breast cancer were recruited for this study, composed of 58 participants with luminal A subtype, 205 participants with luminal B subtype, 66 participants with TNBC subtype, and 79 participants with HER2-enriched subtype. Differences in T stages were observed ($P = .001$; Table 1). A total of 221 participants who underwent neoadjuvant chemotherapy and subsequent surgery were included in the pCR evaluation. The pCR rate was 24.4% (54 of 221), and this variable was associated with estrogen receptor, progesterone receptor, and HER2 status and molecular subtype (all $P < .05$; Table 2).

Table 2: Baseline Characteristics in Participants Who Underwent Neoadjuvant Chemotherapy

Characteristics	pCR (n = 54)	Non-pCR (n = 167)	P Value
Mean age (y)*	51.5 ± 8.4	50.7 ± 8.0	.54[†]
Tumor size (cm)*	3.66 ± 1.87	3.56 ± 1.45	.89[†]
ER			<.001[‡]
Positive	19 (34)	110 (65.9)	...
Negative	35 (66)	57 (34.1)	...
PR			<.001[§]
Positive	1 (7)	72 (43.1)	...
Negative	53 (93)	95 (56.9)	...
HER2			<.001[‡]
Positive	42 (59)	59 (35.3)	...
Negative	12 (41)	108 (64.7)	...
Ki67			.19[‡]
Positive	47 (90)	132 (79.0)	...
Negative	7 (10)	35 (21.0)	...
N stage			.18[‡]
0	5 (9)	19 (11.4)	...
1	22 (41)	46 (27.5)	...
2	16 (30)	74 (44.3)	...
3	11 (20)	28 (16.7)	...
T stage			.14[§]
1	3 (6)	7 (4.2)	...
2	28 (52)	85 (50.9)	...
3	12 (22)	20 (12.0)	...
4	11 (20)	55 (32.9)	...
Molecular subtype			<.001[§]
Luminal A	0 (0)	24 (14.4)	...
Luminal B	19 (35)	86 (51.5)	...
HER2-enriched	27 (50)	30 (18.0)	...
TNBC	8 (15)	27 (16.2)	...

Note.—Unless otherwise indicated, data are numbers of participants; data in parentheses are percentages. ER = estrogen receptor, *HER2* = human epidermal growth factor receptor 2, pCR = pathologic complete response, PR = progesterone receptor, TNBC = triple-negative breast cancer.

* Data are means ± SDs.

[†] Mann-Whitney U test.

[‡] χ^2 test.

[§] Fisher exact test.

Characteristics of Time-Dependent Diffusion MRI–based Microstructural Parameters

Figure 2 shows the dynamic contrast–enhanced MRI scans, ADC maps at different oscillating frequencies, and time-dependent diffusion MRI–fitted microstructural parameter maps in participants with the four subtypes (ie, luminal A, luminal B, TNBC, and *HER2*-enriched subtypes). Quantitatively, Table S1 and Figure 3A show that all time-dependent diffusion MRI microstructural parameters showed differences among four molecular subtypes (all $P < .001$). The luminal B subtype had the lowest ADC and highest cellularity (all adjusted $P < .05$). However, the *HER2*-enriched subtype had the highest ADC value and lowest cellularity (all adjusted $P < .05$). Among them, only cellularity showed differences when comparing the four molecular subtypes in pairs (all adjusted $P < .05$).

Participants with pCR had higher ADC, extracellular diffusivity, and diameter values and lower relative ADC change, intracellular fraction, and cellularity values than participants who did not achieve pCR, based on the pretreatment scans (all $P < .001$; Table S2, Fig 3B).

Univariable and Multivariable Analyses

After adjustment of the multivariable model for the variables with a $P < .05$ at univariable analysis (Table S3), relative ADC change (OR, 0.79; 95% CI: 0.64, 0.98; $P = .03$) and cellularity (OR, 0.58; 95% CI: 0.44, 0.77; $P < .001$) were associated with the luminal A subtype, and only diameter (OR, 4.85; 95% CI: 2.59, 9.09; $P < .001$) was an independent predictor of the luminal B subtype. $ADC_{25\ Hz}$ (OR, 0.58; 95% CI: 0.36, 0.96; $P = .03$) and diameter (OR, 0.42; 95% CI: 0.24, 0.73; $P = .002$) were associated with TNBC, and extracellular diffusivity, cellularity, and diameter (OR, 1.71 [95% CI: 1.02, 2.84; $P = .04$], 1.87 [95% CI: 1.19, 2.95; $P = .007$], and 0.24 [95% CI: 0.11, 0.50; $P <.001$], respectively) were associated with the *HER2*-enriched subtype at multivariable analysis.

Univariable analysis showed that estrogen receptor, progesterone receptor, *HER2* status, and all time-dependent diffusion MRI microstructural parameters were associated with pCR (Table 3). Multivariable analysis demonstrated that progesterone receptor status (OR, 0.08; 95% CI: 0.01, 0.73; $P = .02$), *HER2* status (OR, 3.36; 95% CI: 1.36, 8.31; $P = .009$), and the cellularity index (OR, 0.01; 95% CI: 0.01, 0.52; $P = .02$) were independently associated with pCR.

Performance Evaluation of the Prediction Models

The receiver operating characteristic curves of single time-dependent diffusion MRI microstructural parameters and the corresponding combination models for identifying each molecular subtype are shown in Table S4. Combining relative ADC change and cellularity enabled the identification of the luminal A subtype with the highest AUC among the time-dependent diffusion MRI microstructural parameters, producing an AUC of 0.70 (95% CI: 0.63, 0.75), which was better than that of pulsed gradient spin-echo ADC (AUC, 0.51; 95% CI: 0.47, 0.61) ($P = .003$) (Fig 4A). The AUC of cellularity (AUC, 0.78; 95% CI: 0.73, 0.82) was superior to that of pulsed gradient spin-echo ADC (AUC, 0.70; 95% CI: 0.65, 0.76) ($P < .001$) for identifying the luminal B subtype (Fig 4B). In distinguishing between TNBC and non-TNBC, classification analysis showed that combining $ADC_{25\ Hz}$ and diameter achieved the best performance, with an AUC of 0.72 (95% CI: 0.65, 0.78), which was superior to that of pulsed gradient spin-echo ADC (AUC, 0.59; 95% CI: 0.52, 0.66) ($P < .001$) (Fig 4C). Compared with pulsed gradient spin-echo ADC, the combined model of extracellular diffusivity, cellularity, and diameter showed superior performance in identifying the *HER2*-enriched subtype (AUC, 0.85; 95% CI: 0.80, 0.89) ($P < .001$) (Fig 4D).

For discriminating pCR in response to neoadjuvant chemotherapy, the clinical-pathologic model that combined the progesterone receptor with *HER2* achieved an AUC of 0.79 (95% CI: 0.73, 0.84). Among the time-dependent diffusion MRI microstructural parameters, cellularity achieved the highest AUC (0.84; 95% CI: 0.77, 0.90). Additionally, by integrating
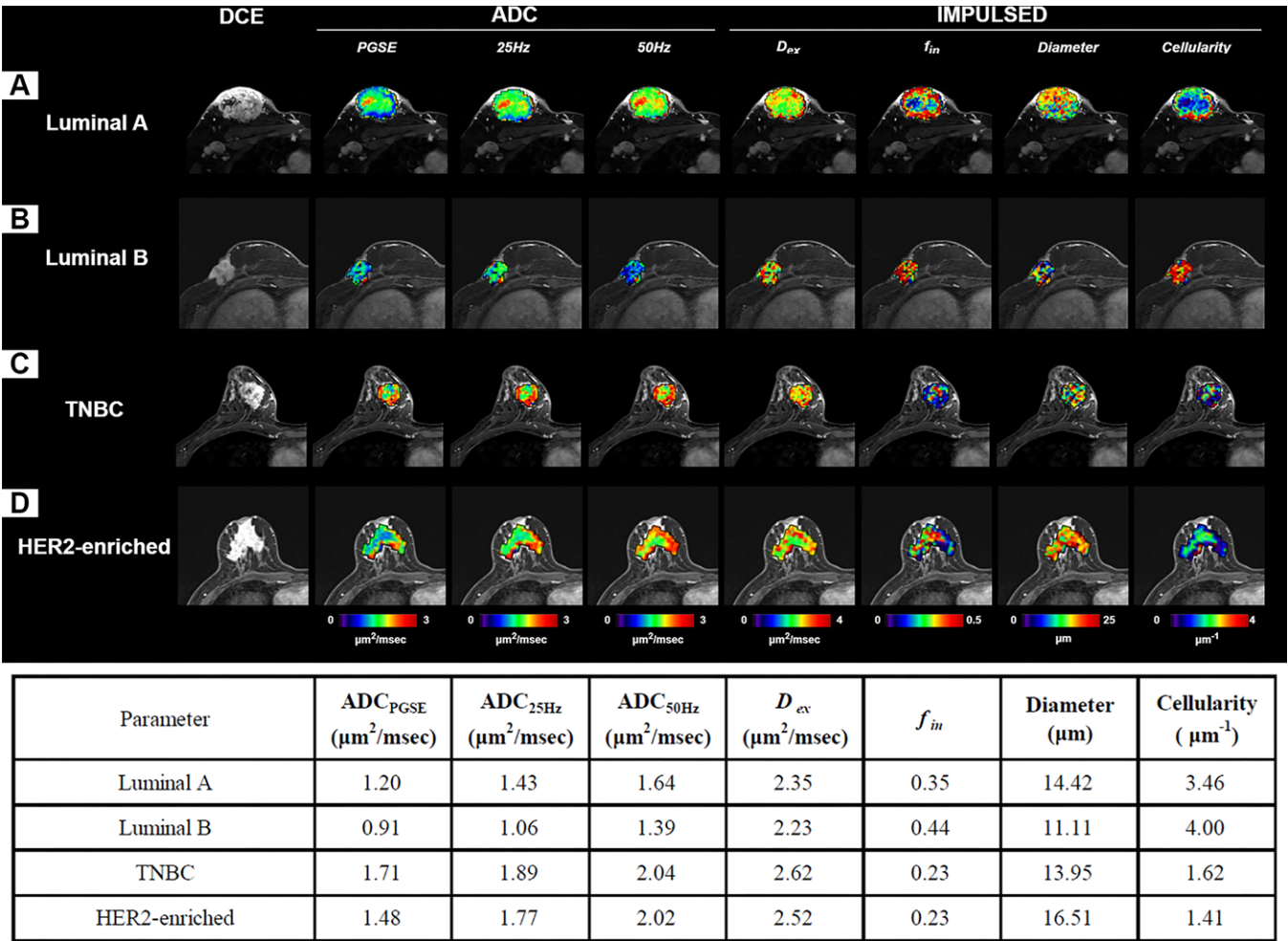
Parameter	ADC_{PGSE} (μm^2/msec)	ADC_{25Hz} (μm^2/msec)	ADC_{50Hz} (μm^2/msec)	D_{ex} (μm^2/msec)	f_{in}	Diameter (μm)	Cellularity (μm^{-1})
Luminal A	1.20	1.43	1.64	2.35	0.35	14.42	3.46
Luminal B	0.91	1.06	1.39	2.23	0.44	11.11	4.00
TNBC	1.71	1.89	2.04	2.62	0.23	13.95	1.62
HER2-enriched	1.48	1.77	2.02	2.52	0.23	16.51	1.41

Figure 2: Diffusivity MRI maps in four participants show pulsed gradient spin-echo (PGSE) and oscillating gradient spin-echo (25 Hz and 50 Hz) data, and microstructural maps, including the extracellular diffusivity (D_{ex})z, intracellular fraction (f_{in}), cell diameter, and cellularity using imaging microstructural parameters with the limited spectrally edited diffusion (IMPULSED) model. The table (bottom) shows the corresponding specific values. **(A)** Diffusivity maps in a 46-year-old woman with stage IIIb luminal A breast cancer who underwent neoadjuvant treatment and did not have pathologic complete response (pCR); the corresponding relative apparent diffusion coefficient (ADC) change was 26.80%. **(B)** Diffusivity maps in a 53-year-old woman with stage IIIb luminal B breast cancer who underwent neoadjuvant treatment and did not have pCR; the corresponding relative ADC change was 34.96%. **(C)** Diffusivity maps in a 44-year-old woman with stage IIIa triple-negative breast cancer (TNBC) who underwent neoadjuvant treatment and had pCR; the corresponding relative ADC change was 16.26%. **(D)** Diffusivity maps in a 64-year-old woman with stage IIIc human epidermal growth factor receptor 2 (HER2)-enriched breast cancer who underwent neoadjuvant treatment and had pCR; the corresponding relative ADC change was 27.04%. ADC_{PGSE} = ADC of pulsed gradient spin-echo data, ADC_{50Hz} = ADC measurement at 50 Hz, ADC_{25Hz} = ADC measurement at 25 Hz, DCE = dynamic contrast enhanced.

clinical-pathologic characteristics with cellularity, the combined model achieved good predictive performance, with an AUC of 0.88 (95% CI: 0.83, 0.93), outperforming conventional ADC measurements and the clinical-pathologic model ($P < .001$) (Table S5, Fig 5). Subgroup analyses based on molecular subtypes are shown in Table S6. Cellularity also achieved the highest AUC in the luminal B subtype (0.78; 95% CI: 0.64, 0.90), TNBC subtype (0.92; 95% CI: 0.77, 1.00), and *HER2*-enriched subtype (0.74; 95% CI: 0.58, 0.85) for prediction of pCR to neoadjuvant chemotherapy.

Validation with Histopathologic Findings
The nuclei of the cells were automatically segmented from the hematoxylin-eosin–stained whole-slide images (Fig 6A–6C). There was a positive correlation between time-dependent diffusion MRI–derived parameters and pathologic measurements in a subset of 100 representative samples (intracellular fraction, $r = 0.81$; diameter, $r = 0.75$; cellularity, $r = 0.67$; all $P < .001$) (Fig 6D, 6F), and negative correlation between pulsed gradient

spin-echo ADC and time-dependent diffusion MRI–derived cellularity and pathologic cellularity ($r = 0.60$ and 0.67, respectively; all $P < .001$) (Fig S2).

Discussion
There is increasing demand for noninvasive prediction of molecular subtypes and pathologic complete response (pCR) in patients with breast cancers. In our study, time-dependent diffusion MRI microstructural parameters demonstrated excellent performance in helping to identify four molecular subtypes (area under the receiver operating characteristic curve [AUC] range, 0.70–0.85), which was better than that of the apparent diffusion coefficient parameters derived from diffusion-weighted imaging. A key finding was that the highest performance for predicting pCR was achieved with a model that combined progesterone receptor, human epidermal growth factor receptor 2–enriched, and cellularity factors (AUC, 0.88). The performance of the model was superior to that of both conventional diffusion MRI (AUC, 0.73; $P < .001$) and the clinical-pathologic model (AUC, 0.79; $P < .001$). The
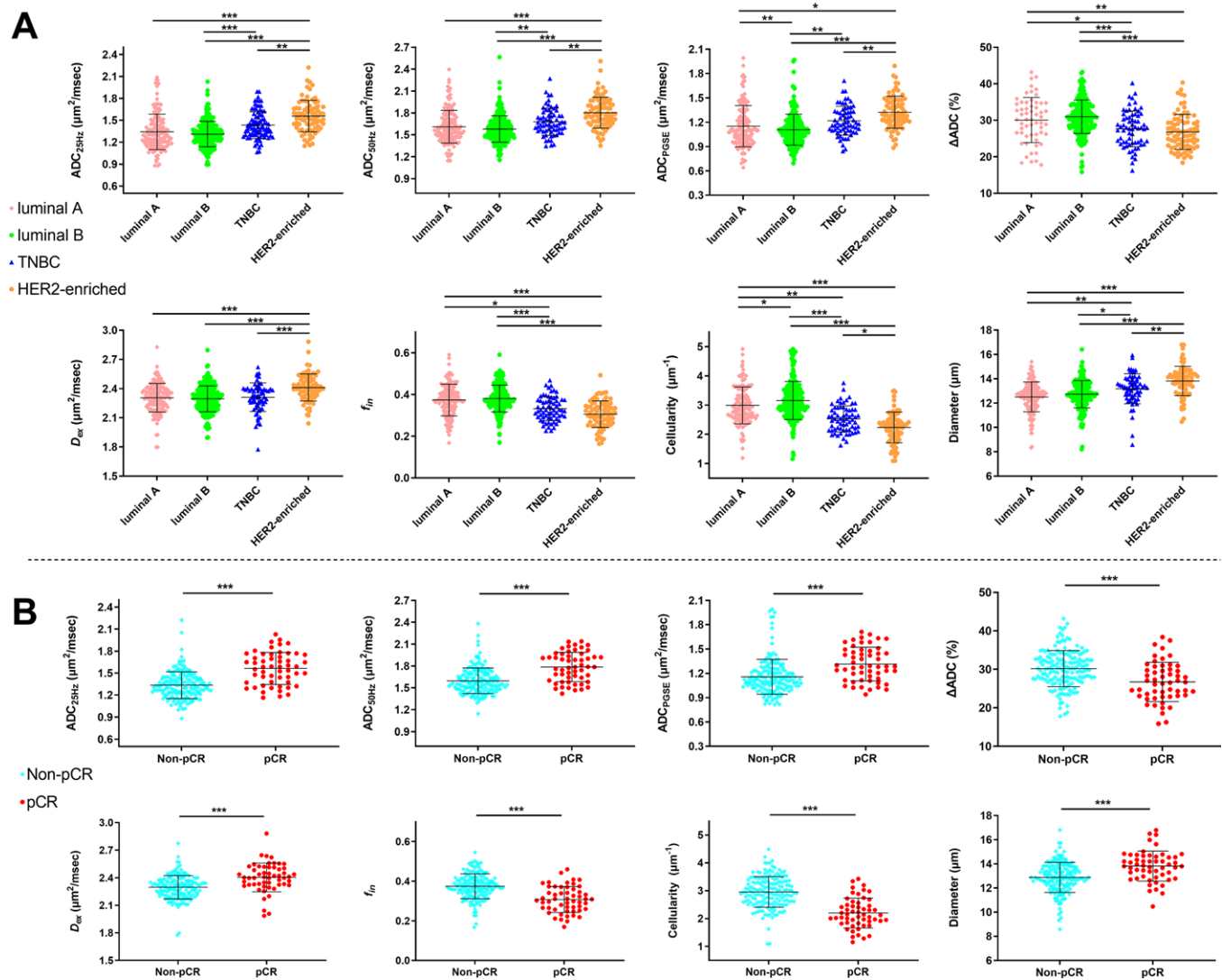
Figure 3: Plots show comparisons of time-dependent diffusion MRI microstructural parameters among molecular subtypes using **(A)** one-way analysis of variance followed by pairwise *t* tests with Bonferroni correction and **(B)** pathologic complete response (pCR) and non-pCR groups using the Mann-Whitney *U* tests. ∗ *P* < .05, ∗∗ *P* < .01, ∗∗∗ *P* < .001. Dots are individual data points, and lines are means ± SDs. ADC = apparent diffusion coefficient, ADC_{PGSE} = ADC of pulsed gradient spin-echo data, ADC_{50Hz} = ADC measurement at 50 Hz, $ADC_{25 Hz}$ = ADC measurement at 25 Hz, D_{ex} = extracellular diffusivity, f_{in} = intracellular fraction, *HER2* = human epidermal growth factor receptor 2, TNBC = triple-negative breast cancer.

time-dependent diffusion MRI–derived microstructural parameters were closely correlated with the pathologic measurements (*r* = 0.67–0.81; *P* < .001).

Morphologic assessments of factors such as the Nottingham grade and histologic subtype provide prognostic information about the clinical manifestations of breast cancer (20). Luminal B cancers have a worse prognosis than luminal A cancers and often have higher Nottingham grades and higher proliferation rates (21), resulting in higher cellularity. We confirmed this by using time-dependent diffusion MRI–derived cellularity. The *HER2*-enriched subtype is typically categorized at histologic analysis as a high-grade subtype with apocrine characteristics, exhibiting notable attributes such as large cell volume, abundant eosinophilic and granular cytoplasm, a large nucleus, and prominent nucleoli (22). We demonstrated that the *HER2*-enriched subtype had the largest cell diameter using the non-invasive time-dependent diffusion MRI method. TNBC is a subtype with high heterogeneity, and the microstructural parameters at time-dependent diffusion MRI show moderate

effectiveness. This may be related to the characteristic histologic features of TNBC such as solid-pushing borders, geographic areas of necrosis, central fibrous lesions, and dense lymphocytic infiltrates (22).

We demonstrated clear differences in time-dependent diffusion MRI microstructural parameters among molecular subtypes (AUC range, 0.70–0.85), comparable to the results obtained using parameters derived from intravoxel incoherent motion (AUC range, 0.60–0.86) (23) and slightly better than those derived from diffusion-kurtosis imaging–derived parameters (AUC range, 0.50–0.78) (24). At breast cancer imaging, the perfusion fraction typically approximates 0.1 (25), and pseudodiffusivity generally exceeds the tissue ADC by an order of magnitude (26). When considering *b* values greater than 250 sec/mm², the proportion of the attenuated intravoxel incoherent motion signal to the total signal was calculated to be less than 0.74%. Therefore, the cell modeling in our study neglected the intravoxel incoherent motion effect for more robust estimates of microstructural parameters. Although more work is needed before it can replace

Table 3: Univariable and Multivariable Analyses of the Associations of Time-Dependent Diffusion MRI–Derived Microstructural Measures with Pathologic Complete Response

	Univariable Analysis		Multivariable Analysis		
Predictor	OR	*P* Value	β Coefficient	OR	*P* Value
Clinical-pathologic characteristic					
Age	0.91 (0.67, 1.23)	.53	...	...	...
ER					
Negative	Reference	...	...	...	
Positive	0.28 (0.15, 0.54)	<.001	0.74	2.10 (0.81, 5.47)	.13
PR					
Negative	Reference	...	...	...	
Positive	0.02 (0.01, 0.18)	<.001	−2.50	0.08 (0.01, 0.73)	.02
HER2					
Negative	Reference	...	...	...	
Positive	6.41 (3.13, 13.11)	<.001	1.21	3.36 (1.36, 8.31)	.009
Ki67					
Negative	Reference	...	...	...	...
Positive	1.78 (0.74, 4.30)	.19	...	...	...
N stage					
0	Reference	...	...	...	...
1	1.81 (0.95, 2.43)	.07	...	...	...
2	0.53 (0.27, 1.02)	.06	...	...	...
3	1.27 (0.58, 2.76)	.55	...	...	...
T stage					
1	Reference	...	...	...	...
2	1.04 (0.56, 1.92)	.90	...	...	...
3	0.9 (0.38, 2.12)	.67	...	...	...
4	4.57 (2.35, 8.87)	.83	...	...	...
Time-dependent diffusion MRI microstructural parameters					
$ADC_{25\,Hz}$	3.27 (2.20, 4.86)	<.001	0.77	2.17 (0.26, 17.84)	.47
$ADC_{50\,Hz}$	2.71 (1.89, 3.88)	<.001	−0.42	0.65 (0.06, 6.61)	.72
ADC_{PGSE}	1.97 (1.43, 2.70)	<.001	−0.47	0.63 (0.09, 4.18)	.63
Relative ADC change	0.47 (0.33, 0.67)	<.001	−0.04	0.97 (0.31, 3.02)	.95
Extracellular diffusivity	2.42 (1.65, 3.55)	<.001	0.28	1.33 (0.60, 2.93)	.50
Intracellular fraction	0.33 (0.22, 0.49)	<.001	2.38	10.83 (0.56, 208.90)	.12
Cellularity	0.20 (0.12, 0.33)	<.001	−4.22	0.01 (0.01, 0.52)	.02
Diameter	2.33 (1.59, 3.42)	<.001	−1.18	0.31 (0.08, 1.15)	.08

Note.—Data in parentheses are 95% CIs. ADC = apparent diffusion coefficient, $ADC_{50\,Hz}$ = ADC measurement at 50 Hz, ADC_{PGSE} = pulsed gradient spin-echo ADC, $ADC_{25\,Hz}$ = ADC measurement at 25 Hz, ER = estrogen receptor, *HER2* = human epidermal growth factor receptor 2, OR = odds ratio, PR = progesterone receptor, TNBC = triple-negative breast cancer.

invasive immunohistochemistry detection methods, it provides a noninvasive way to view patterns of microstructural features related to molecular subtypes and can be used to assist personalized treatment strategies (15). Further investigation is needed to assess the use of its application within the context of contrast-unenhanced MRI and if dynamic contrast-enhanced MRI is unavailable or unsuitable (27).

Cellularity was a crucial marker among time-dependent diffusion MRI microstructural parameters and showed the highest performance in predicting pCR (AUC, 0.84), which was superior to that of the ADC measurements and the clinical-pathologic model. Additionally, by combining the cellularity, progesterone receptor, and *HER2* variables, the model performance (AUC, 0.88) improved. Therefore, clinical-pathologic information offers more incremental benefits. Studies (28–30) have been variable

regarding the use of ADC in predicting pCR. Eun et al (31) used pretreatment ADC mapping texture analysis to predict pCR and achieved AUCs ranging from 0.52 to 0.57. A meta-analysis (30) concluded that diffusion-weighted imaging could help to accurately assess the pCR to neoadjuvant chemotherapy in individuals with breast cancer (AUC, 0.82; 95% CI: 0.79, 0.85). Nonetheless, further investigations with well-designed, large-scale, multicenter clinical trials are needed. Another study (32) integrated imaging features and molecular subtypes to construct models for predicting pCR, which achieved AUCs ranging from 0.83 to 0.87 and showed a performance that was comparable to our study.

Notably, compared with artificial intelligence analysis methods, the time-dependent diffusion MRI model is biophysically supported, explainable, and clinically feasible. We used simple
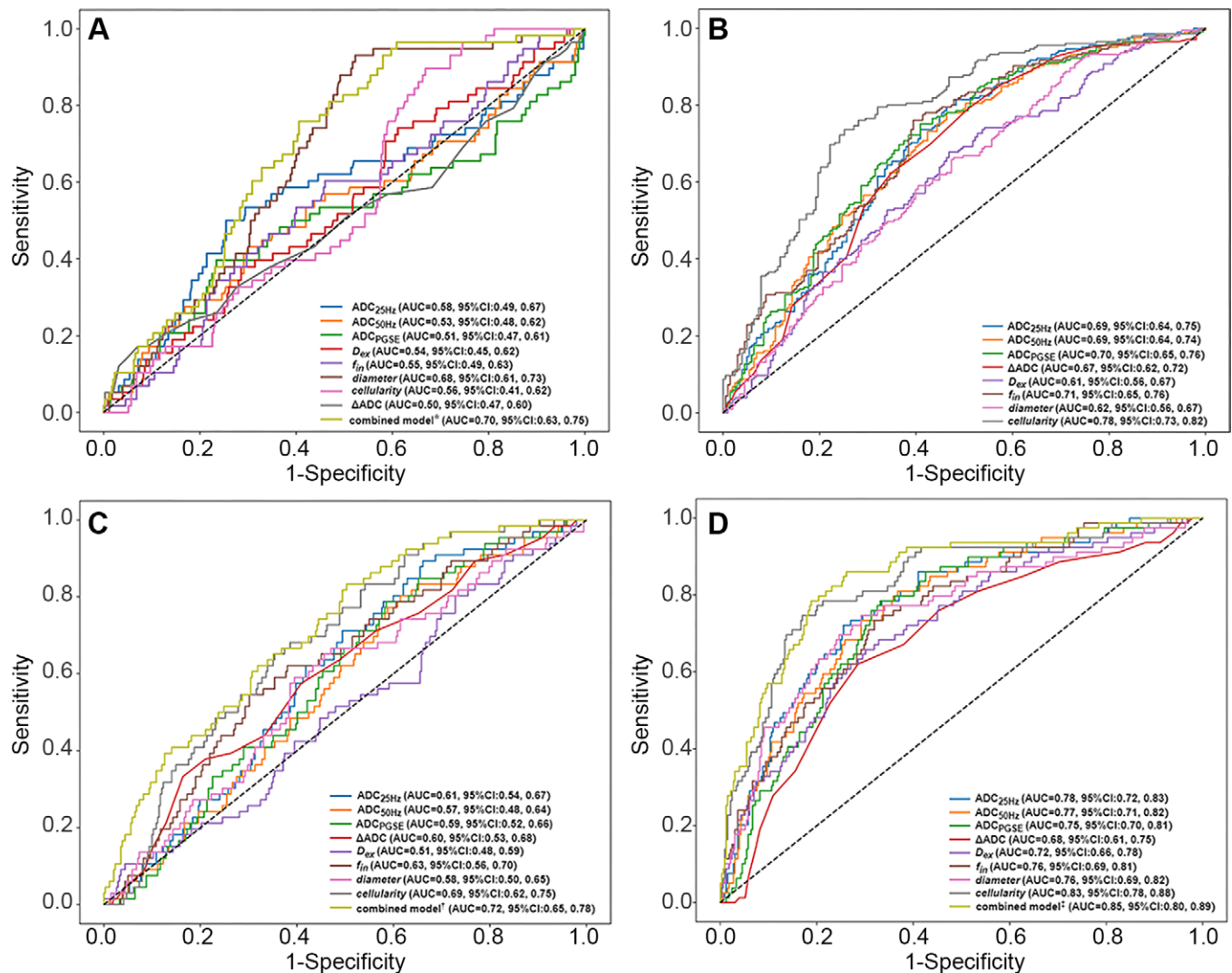
Figure 4: Receiver operating characteristic curves show the single time-dependent diffusion MRI microstructural parameter and combined models (and multivariable analysis show independent predictors) in participants with **(A)** luminal A, **(B)** luminal B, **(C)** triple-negative breast cancer, **(D)** and human epidermal growth factor receptor 2–enriched subtypes. * Combined relative ADC change (ΔADC) and cellularity. † Combined apparent diffusion coefficient (ADC) measured at 25 Hz (ADC$_{25 Hz}$) and diameter. ‡ Combined extracellular diffusivity, cellularity, and diameter. ADC$_{50 Hz}$ = ADC measured at 50 Hz, ADC$_{PGSE}$ = ADC of pulsed gradient spin-echo data, AUC = area under the receiver operating characteristic curve, D_{ex} = extracellular diffusivity, f_{in} = intracellular fraction.

averages over each region of interest and logistic regression to avoid overfitting. The time-dependent diffusion MRI microstructural parameters were highly correlated with pathologic examination–based microstructural properties (r = 0.67–0.81). Higher cellularity in tumors is associated with increased proliferation and invasiveness, leading to lower chances of achieving pCR to neoadjuvant chemotherapy. Hence, this approach is highly generalizable and has high potential for wide application in the clinical treatment of breast tumors. In our study, pulsed gradient spin-echo ADC had correlation strength with pathologic cellularity similar to time-dependent diffusion MRI–derived cellularity. A moderate correlation was found between pulsed gradient spin-echo ADC and time-dependent diffusion MRI–derived cellularity, indicating that they are not completely identical and could complement each other.

Our study had several limitations. First, this was only a single-center exploratory study; multicenter studies are necessary to validate our conclusions in the future. Second, the regions of interest were manually defined; automated tumor segmentation

methods may reduce the interoperator variability and improve the accuracy. Third, time-dependent diffusion MRI microstructural parameters were averaged over a single region of interest on the tumor, ignoring intratumoral heterogeneity. In the future, intratumoral heterogeneity analysis should be performed. Fourth, intravoxel incoherent motion effects can introduce variability in diffusion MRI signals, particularly at low b values, and these effects may differ between sequences such as pulsed gradient spin echo and oscillating gradient spin echo, potentially confounding the interpretation of our findings. Although relatively high b values were used in this study, future research could benefit from explicitly modeling intravoxel incoherent motion effects to provide a more accurate assessment of microstructural properties. Furthermore, histopathologic slides were obtained by sampling a limited area of the tumor, whereas time-dependent diffusion MRI microstructural parameters were derived from the entire tumor region, leading to a lack of precise matching. Finally, we did not combine time-dependent diffusion MRI microstructural parameters with other multiparametric
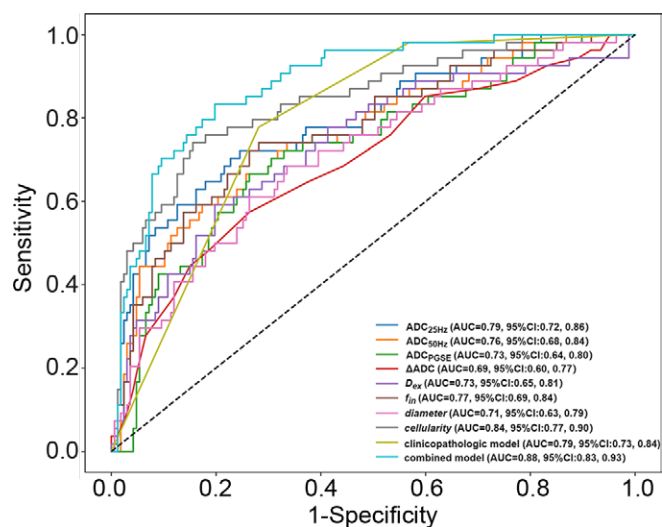
Figure 5: Receiver operating characteristic curves show individual time-dependent diffusion MRI microstructural parameters, the clinical-pathologic model (progesterone receptor and human epidermal growth factor receptor 2 [HER2]), and the combined model (progesterone receptor, HER2, and cellularity) for predicting pathologic complete response. ADC = apparent diffusion coefficient, ΔADC = relative ADC change, $ADC_{50\ Hz}$ = ADC measurement at 50 Hz, $ADC_{25\ Hz}$ = ADC measurement at 25 Hz, AUC = area under the receiver operating characteristic curve, D_{ex} = extracellular diffusivity, f_{in} = intracellular fraction.

MRI scans, which could have provided more detailed information about the markers of cancer and may further improve the prediction performance.

In summary, we demonstrated the clinical value of time-dependent diffusion MRI microstructural parameters in predicting molecular subtypes and pathologic complete response (pCR) in patients with breast cancers. Different molecular subtypes exhibit unique microstructural properties, and the combination of progesterone receptor, human epidermal growth factor receptor 2, and cellularity (an imaging-based marker) achieved the best performance for predicting pCR. In the future, efforts will be made to address these limitations and validate the research findings by using larger cohorts and multiple centers.

Deputy Editor: Linda Moy
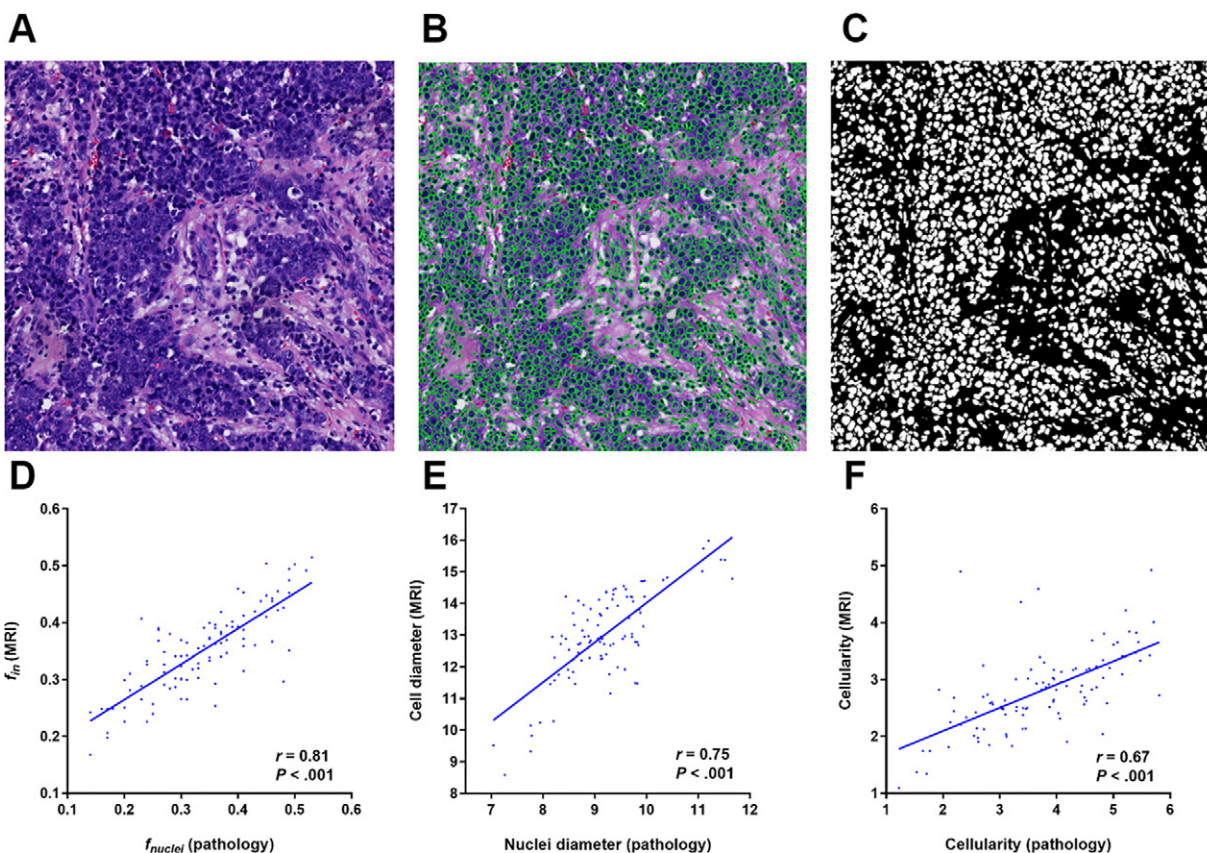**Scientific Editor:** Shannyn Wolfe (AJE)

Figure 6: The correlations between time-dependent diffusion MRI–derived microstructural parameters and results of pathologic examination–based microstructural properties (n = 100). **(A)** Hematoxylin-eosin–stained image (magnification, ×40) shows pathologic specimens from one participant. **(B)** Hematoxylin-eosin–stained image (magnification, ×40) shows nuclei that were segmented by a pretrained conditional generative adversarial network, and **(C)** the pathologic microstructural properties were automatically quantified. The graph shows the correlations between the **(D)** time-dependent diffusion MRI-derived intracellular fraction (f_{in}), **(E)** diameter, and **(F)** cellularity and the pathologic examination–based microstructural properties. f_{nuclei} = nuclei fraction.

References

1. Harbeck N, Penault-Llorca F, Cortes J, et al. Breast cancer. Nat Rev Dis Primers 2019;5(1):66.
2. Tan PH, Ellis I, Allison K, et al; WHO Classification of Tumours Editorial Board. The 2019 World Health Organization classification of tumours of the breast. Histopathology 2020;77(2):181–185.
3. De Mattos-Arruda L, Shen R, Reis-Filho JS, Cortés J. Translating neoadjuvant therapy into survival benefits: one size does not fit all. Nat Rev Clin Oncol 2016;13(9):566–579.
4. Reig B, Lewin AA, Du L, et al. Breast MRI for Evaluation of Response to Neoadjuvant Therapy. RadioGraphics 2021;41(3):665–679.
5. Amornsiripanitch N, Bickelhaupt S, Shin HJ, et al. Diffusion-weighted MRI for Unenhanced Breast Cancer Screening. Radiology 2019;293(3):504–520.
6. Kazama T, Takahara T, Hashimoto J. Breast Cancer Subtypes and Quantitative Magnetic Resonance Imaging: A Systemic Review. Life (Basel) 2022;12(4):490.
7. Suo S, Yin Y, Geng X, et al. Diffusion-weighted MRI for predicting pathologic response to neoadjuvant chemotherapy in breast cancer: evaluation with mono-, bi-, and stretched-exponential models. J Transl Med 2021;19(1):236.
8. Zhang H, Liu K, Ba R, et al. Histological and molecular classifications of pediatric glioma with time-dependent diffusion MRI-based microstructural mapping. Neuro Oncol 2023;25(6):1146–1156.
9. Reynaud O. Time-Dependent Diffusion MRI in Cancer: Tissue Modeling and Applications. Front Phys 2017;5:58.
10. Jiang X, Li H, Xie J, Zhao P, Gore JC, Xu J. Quantification of cell size using temporal diffusion spectroscopy. Magn Reson Med 2016;75(3):1076–1085.
11. Jiang X, Li H, Xie J, et al. In vivo imaging of cancer cell size and cellularity using temporal diffusion spectroscopy. Magn Reson Med. 2017;78(1):156–164.
12. Xu J, Jiang X, Li H, et al. Magnetic resonance imaging of mean cell size in human breast tumors. Magn Reson Med 2020;83(6):2002–2014.
13. Ba R, Wang X, Zhang Z, et al. Diffusion-time dependent diffusion MRI: effect of diffusion-time on microstructural mapping and prediction of prognostic features in breast cancer. Eur Radiol 2023;33(9):6226–6237.
14. Jiang XY, McKinley ET, Xie JP, Gore JC, Xu JZ. Detection of Treatment Response in Triple-Negative Breast Tumors to Paclitaxel Using MRI Cell Size Imaging. J Magn Reson Imaging 2024;59(2):575–584.
15. Wu D, Jiang K, Li H, et al. Time-Dependent Diffusion MRI for Quantitative Microstructural Mapping of Prostate Cancer. Radiology 2022;303(3):578–587.
16. Iima M, Yamamoto A, Kataoka M, et al. Time-dependent diffusion MRI to distinguish malignant from benign head and neck tumors. J Magn Reson Imaging 2019;50(1):88–95.
17. Perou CM, Sørlie T, Eisen MB, et al. Molecular portraits of human breast tumours. Nature 2000;406(6797):747–752.
18. Wolff AC, Hammond MEH, Hicks DG, et al; College of American Pathologists. Recommendations for human epidermal growth factor receptor 2 testing in breast cancer: American Society of Clinical Oncology/College of American Pathologists clinical practice guideline update. J Clin Oncol 2013;31(31):3997–4013.
19. Isola P, Zhu JY, Zhou T, Efros AA. Image-to-Image Translation with Conditional Adversarial Networks. 2017 IEEE Conference on Computer Vision and Pattern Recognition (CVPR), Honolulu, HI: 5967–5976
20. Wang Y, Acs B, Robertson S, et al. Improved breast cancer histological grading using deep learning. Ann Oncol 2022;33(1):89–98.
21. Cheang MCU, Chia SK, Voduc D, et al. Ki67 index, HER2 status, and prognosis of patients with luminal B breast cancer. J Natl Cancer Inst 2009;101(10):736–750.
22. Allison KH. Molecular pathology of breast cancer: what a pathologist needs to know. Am J Clin Pathol 2012;138(6):770–780.
23. Zhao M, Fu K, Zhang L, et al. Intravoxel incoherent motion magnetic resonance imaging for breast cancer: A comparison with benign lesions and evaluation of heterogeneity in different tumor regions with prognostic factors and molecular classification. Oncol Lett 2018;16(4):5100–5112.
24. Kang HS, Kim JY, Kim JJ, et al. Diffusion Kurtosis MR Imaging of Invasive Breast Cancer: Correlations With Prognostic Factors and Molecular Subtypes. J Magn Reson Imaging 2022;56(1):110–120.
25. Arian A, Seyed-Kolbadi FZ, Yaghoobpoor S, Ghorani H, Saghazadeh A, Ghadimi DJ. Diagnostic accuracy of intravoxel incoherent motion (IVIM) and dynamic contrast-enhanced (DCE) MRI to differentiate benign from malignant breast lesions: A systematic review and meta-analysis. Eur J Radiol 2023;167:111051.
26. Liang J, Zeng S, Li Z, et al. Intravoxel Incoherent Motion Diffusion-Weighted Imaging for Quantitative Differentiation of Breast Tumors: A Meta-Analysis. Front Oncol 2020;10:585486.
27. Baltzer P, Mann RM, Iima M, et al; EUSOBI international Breast Diffusion-Weighted Imaging working group. Diffusion-weighted imaging of the breast-a consensus and mission statement from the EUSOBI International Breast Diffusion-Weighted Imaging working group. Eur Radiol 2020;30(3):1436–1450.
28. Partridge SC, Zhang Z, Newitt DC, et al; ACRIN 6698 Trial Team and I-SPY 2 Trial Investigators. Diffusion-weighted MRI Findings Predict Pathologic Response in Neoadjuvant Treatment of Breast Cancer: The ACRIN 6698 Multicenter Trial. Radiology 2018;289(3):618–627.
29. Mendez AM, Fang LK, Meriwether CH, et al. Diffusion Breast MRI: Current Standard and Emerging Techniques. Front Oncol 2022;12:844790.
30. Li Z, Li J, Lu X, Qu M, Tian J, Lei J. The diagnostic performance of diffusion-weighted imaging and dynamic contrast-enhanced magnetic resonance imaging in evaluating the pathological response of breast cancer to neoadjuvant chemotherapy: A meta-analysis. Eur J Radiol 2021;143:109931.
31. Eun NL, Kang D, Son EJ, et al. Texture Analysis with 3.0-T MRI for Association of Response to Neoadjuvant Chemotherapy in Breast Cancer. Radiology 2020;294(1):31–41.
32. Shi Z, Huang X, Cheng Z, et al. MRI-based Quantification of Intratumoral Heterogeneity for Predicting Treatment Response to Neoadjuvant Chemotherapy in Breast Cancer. Radiology 2023;308(1):e222830.